International Journal of Multiphysics
Volume 18, No. 2, 2024
ISSN: 1750-9548

Enhancing Accuracy in Wind and Photovoltaic Power Forecasting Through Neutral Network and Beluga Whale Optimization Algorithm

Peng Chen[1,*], Panpan Liu[1], Li Lan[1], Mingxing Guo[1], Hongyu Guo[2]

[1]State Grid Shanghai Power Company Economic and Technical Research Institute, Shanghai, China

[2]Shanghai University of Electric Power, Shanghai, China

*Corresponding Author.

Abstract

As the total energy consumption continues to rise, environmental issues and the balance of energy supply and demand have become increasingly severe. With the integration of photovoltaic and wind power generation, wind and solar power generation, while reducing users' carbon emissions, also introduce additional complexity to the power system due to their inherent uncertainty. However, deep learning algorithms have shown tremendous potential in accurately predicting wind and solar power output. This paper combinate the ICEEMDAN algorithm and temporal convolutional neural network to achieve dynamic forecasting of wind and photovoltaic power outputs. In addition, an enhanced beluga whale optimization algorithm is utilized to select optimal hyperparameter combinations for the forecasting model, so that the accuracy and robustness of the model's forecasting outcomes can be enhanced. The research results show that the wind and photovoltaic power forecasting model we constructed can effectively mitigates the impact of volatility and complexity associated with these energy sources on prediction outcomes and achieve accurate forecasting.

Keywords: Wind and photovoltaic power forecasting, correlation analysis, deep learning, neutral network, beluga whale optimization algorithm (BWO).

1. Introduction

Currently, wind power generation has become a significant component of China's energy structure. Wind energy, as a typical environmentally friendly power source, possesses advantages such as renewability and no greenhouse gas emissions [1]. However, because of the stochastic and fluctuating nature of [2], integrating wind power into the grid for effective frequency regulation remains challenging. Consequently, enhancing the accuracy of forecasting is a momentous research direction [3,4].

The previously employed wind-solar complementary power generation systems simply combined wind and solar energy production equipment. Due to their small size and lack of specific computational models, their utility was quite limited. The progression of wind-solar hybrid power generation systems in China has advanced through three stages: small-scale standalone integrated wind power systems, grid-based decentralized small-scale wind-solar power systems, and long-distance solar power generation systems. Large-scale wind-solar complementary power generation systems connect independent wind power plants and separate photovoltaic power plants over long distances. Most of these systems fall into the megawatt category, and they face challenges such as high penetration rates when connected to the grid [5]. Fluctuations in the overall processing capacity can negatively impact the safety and stability of grid operations [6].

To address the challenges mentioned above, domestic and international scholars have conducted a series of studies. The combination of wind and solar hybrid energy production with computational methods, especially

methods in the field of deep learning, is significantly influencing the landscape of wind and solar power output prediction [7,8]. The analytical power of computational analysis is widely used to improve the stability and precision of power prediction models. With the emergence of complex deep learning algorithms, researchers can extract satisfactory solutions from large amounts of data, thereby predicting wind power generation more accurately and efficiently. Ding et al. [9] established a dynamic analysis model and applied the active and reactive power decoupling dual-loop current control strategy to wind and photovoltaic power generation systems. They introduced a novel maximum power tracking algorithm. António et al. [10] systematically selecting meteorological features to minimize wind power prediction errors through a sequential forward feature selection algorithm. With the analysis of seven wind plants in Portugal with distinct climates, it was observed that this method significantly reduced the root mean square error of the power prediction results. Ye et al. [11] introduced a novel prediction model for hybrid wind power. They increased the importance of the neural network using the multi-objective Runge-Kutta algorithm (MORUN), thus enhancing prediction accuracy and stability. To further improve the model's predictive ability, integrated learning strategies were also added. Yang et al. [12] presented a wind farm forecasting model utilizing a nonlinear mapping network. The meteorological data of the Numerical Weather Forecasting (NWF) system is incorporated into this model as external components, allowing it to acquire the underlying patterns of wind power generation time series. By balancing the internal factors of wind farm time series data and the external factors of meteorological data, the issue of wind farm curtailment could be effectively addressed. Wang et al. [13] proposed a neural network model to forecast wind power. This method utilizes the asymmetric Laplace distribution to describe the uncertainty of wind power generation forecasts, enabling more precise and reliable interval forecasting outcomes. Wang et al. [14] proposed a novel ensemble probabilistic predicting model. It selects the optimal model input for predicting wind power generation based on the maximal information coefficient values. Wang et al. [15] introduced a method that combines prior guidance with data-driven approaches to deliver accurate and meaningful wind farm predictions. The model's performance was validated using both real-world datasets and publicly available datasets.

With the escalating concern over environmental pollution, solar energy has gained significant attention in recent years as an optimal clean energy source. Similar to wind power, accurate prediction of photovoltaic power holds paramount importance for the secure and steady operation of the power system [16]. With the different methods of power forecasting, we can distinguish between two primary methodologies: direct prediction and indirect prediction. Direct prediction involves employing forecasting models to directly predict photovoltaic power output. On the other hand, indirect prediction entails precise forecasting of solar radiation quantity and combining it with the photovoltaic power calculation formula to achieve photovoltaic power prediction.

In terms of direct prediction methods, Yin et al. [17] constructed the photovoltaic power prediction model by combining particle swarm optimization with machine learning algorithms, effectively reducing the prediction error. Li et al. [18] presented a multi-factor photovoltaic power prediction model incorporating fuzzy C-means, improved white shark optimizer, error correction, variational mode decomposition and long short-term memory. This innovative model substantially enhances photovoltaic power prediction accuracy, mitigating the impact of photovoltaic data volatility on predictive outcomes. In the domain of indirect prediction methods, scholars worldwide have extensively researched solar radiation forecasting methods. The HOTTEL and ASHRAE models are two internationally recognized approaches. Liu et al. [19] established a random forest classifier based on factors influencing solar radiation, creating a random forest-based solar radiation prediction model. Xin et al. [20] explored a novel computational intelligence model, a hybrid of extreme gradient boosting (XGB), covariance matrix adaptation evolutionary strategy (CMAES), and multi-adaptive regression splines (MARS), for precise predicting of daily-scale solar radiation. Sharma et al. [21] introduced a novel approach for solar radiation forecasting, achieving hourly forecasts using a mixed wavelet neural network (WNN). Sun et al. [22] established a solar radiation illuminance prediction system using an improved fruit fly algorithm, planning node locations correlated with solar radiation illuminance behavior. Goliatt et al. [23], drawing from stochastic modeling theory, proposed a solar radiation value prediction model, generating prediction intervals and expected values under varying cloud cover conditions. Model validation using data from a US BMS photovoltaic power station demonstrated the model's commendable predictive accuracy.

According to the above research, in the wind and photovoltaic power generation forecasts, employing techniques such as data decomposition and heuristic algorithm optimization can enhance the accuracy of predictions for both wind and photovoltaic power outputs. Additionally, the utilization of correlation analysis algorithms proves effective in mitigating the influence of weakly correlated components on predictive outcomes. Moreover, the application of error correction models contributes importantly to enhancing the precision of renewable energy power forecasts.

The remainder of this paper is structed as follows: Section 2 procides the methodology; Section 3 outlines the data and results; Section 4 presents the conclusions of this work.

2. Methodology

2.1 Factors influencing model forecasting accuracy

To enhance both training efficiency and predictive precision of the model, it is imperative to incorporate highly correlated influential factors as input parameters in the deep learning model, thereby mitigating the impact of weakly correlated factors on training outcomes [24,25]. In this study, considerations are directed towards meteorological factors, geographical factors, historical wind and solar power data, and other pertinent aspects, as shown in Table 1, illustrating the primary influencing factors.

Based on the influencing factors listed in Table 1, the relationship between every influencing factor and wind and photovoltaic power can be calculated using the correlation analysis method. The calculation formula is presented in Equation (1).

Table 1 Influential factors in the power forecasting model.

Types	Wind power forecasting model	Photovoltaic power forecasting model
Factors	Environmental temperature Soil temperature Air specific humidity Intensity of solar radiation Wind speed at 10 meters Wind speed at 50 meters Historical wind power	Environmental temperature Soil temperature Air specific humidity Intensity of solar radiation Wind speed at 10 meters Wind speed at 50 meters Historical photovoltaic power
Output results	Wind power	Photovoltaic power

$$\rho_{xy} = \frac{\sum_{i=1}^{N}(x_i - \bar{x})(y_i - \bar{y})}{\sqrt{\sum_{i=1}^{N}(x_i - x)^2}\sqrt{\sum_{i=1}^{N}(y_i - y)^2}} \#(1)$$

Here, ρ_{xy} represents the correlation coefficient between time series x and y; N denotes the number of data points in the time series; $\bar{x}$ signifies the mean value of the time series x_i, while $\bar{y}$ signifies the mean value of y_i. The value range of ρ_{xy} lies between [-1, 1], with $|\rho_{xy}|$ reflecting the strength of correlation between the data. A higher $|\rho_{xy}|$ value signifies stronger correlation. Specifically, $\rho_{xy}=0$ indicates no correlation between two variables, $|\rho_{xy}| < 0.3$ suggests weak correlation, $0.3 < \rho_{xy} < 0.5$ indicates moderate correlation, and $|\rho_{xy}| > 0.5$ implies strong correlation.

2.2 The forecasting model

2.2.1 Methodology to preprocess input data in the forecasting model.

Currently, the CEEMDAN algorithm is commonly used for analyzing non-stationary and nonlinear data parameters in time-domain analysis [26,27]. This algorithm addresses the issues of error caused by overlapping signals and low computational efficiency in the EEMD algorithm [28-30], and CEEMDAN also alleviates the phenomenon of mode mixing to some extent. Despite these improvements, the CEEMDAN algorithm still has areas that require enhancement: *(a)* residual noise remains present in the modes, and *(b)* the appearance of signal information occurs later compared to EEMD, with some 'pseudo' patterns emerging during early stages of decomposition. The Improved CEEMDAN (ICEEMDAN) algorithm partially resolves these challenges.

Accurate short-term forecasting of multivariate load data is the basis for the operation and optimization of integrated energy systems, bearing significant importance in the analysis and study of system demand-side dynamics [31,32]. Long Short-Term Memory (LSTM) neural networks [33], a form of deep learning algorithm, are extensively utilized in load forecasting due to their advantages in modeling complex data patterns and analyzing temporal correlations in data.

As an enhancement algorithm for recurrent neural networks (RNNs), LSTM neural network not only has the ability of RNN's efficient processing of load data, time, and to solve the problems of RNN gradient disappearance, explosion, etc., but also has the characteristic of strong processing capacity and high efficiency [34,35].

Compared to the classical RNN, LSTM neural network adds a "processor" called a cell on top of it, which is used to determine whether the information is useful. Within a cell, there are three gates: the input gate i_t, the output gate o_t and the forget gate f_t. When information is put into the LSTM network, the three control gates within the cell manage the selection of memory feedback and adjust the parameters for gradient descent to optimize the self-loop weights, ensuring dynamic changes in weights. The structure is depicted in Figure 1, where the output of LSTM at moment t is x_t, the input value is h_t, and the memory state is c_t.

According to the structure shown in Figure 1, when the data h_{t-1} of the current time period is passed in with the time period implicit layer and the input data x_t of the current time after passing through f_t, irrelevant information is discarded. The calculation formula as shown in Equation (2).

$$f_t = \sigma(W_f \cdot [h_{t-1}, x_t] + b_f) \#(2)$$

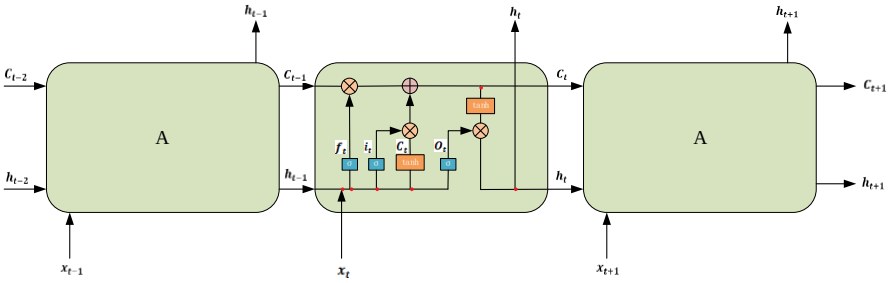

Figure 1 LSTM structure

where σ is the activation function; W_f and b_f are the weight matrix and bias vector in the forget gate f_t, respectively.

The new information is then computed by the activation function (sigmoid function), which is solved to obtain data that can be put into the memory cell, while a new alternate state $\widetilde{C_t}$ is acquired by the tanh functionand at the same time, which is calculated by Equations (3) and (4):

$$i_t = \sigma(W_i \cdot [h_{t-1}, x_t] + b_i) \#(3)$$

$$\widetilde{C_t} = \tanh(W_c \cdot [h_{t-1}, x_t] + b_c) \#(4)$$

where W_i and b_i are the weight matrix and bias vector in the input gate, respectively; W_c and b_c are the weight matrix and bias vector in the cell state, respectively. Then the value of the cell state at the current time is given by Equation (5).

$$C_t = \sigma f_t C_{t-1} + i_t \widetilde{C_t} \#(5)$$

Additionally, by applying the tanh function to the data o_t classified through the sigmoid function and the new cell state C_t, the value h_t of the hidden layer data to be passed in the next time step is obtained, as shown in Equations (6) and (7):

$$o_t = \sigma(W_o \cdot [h_{t-1}, x_t] + b_o) \#(6)$$

$$h_t = o_t \tanh(C_t) \#(7)$$

where W_o and b_o are the weight matrix and bias vector of the output gate.

2.2.2 Improved beluga whale optimization algorithm - hyperparameter optimization

As a new optimization algorithm. The beluga whale optimization algorithm (BWO) is inspired by beluga whales, simulating their swimming, foraging, and "whale fall" behaviors [36]. The BWO algorithm consists of two phases: exploration and exploitation. The exploitation phase manages local search within the same area, whereas the exploration phase employs random selection to guarantee global search capability in the design space. The behavior of beluga whales is represented as that of a search agent capable of navigating the search space by adjusting its position vector [37]. Moreover, BWO also takes into account the likelihood of a whale fall. Due to its population-based mechanism, every beluga whale in the BWO algorithm represents a candidate solution and undergoes continuous updates throughout the optimization process [38,39].

Although the BWO algorithm has the above advantages, most of them use random initialization to generate the initial population in the initial stage, which complicates the task of maintaining population diversity throughout the entire optimization process. To solve the problems above, we introduces the opposites learning mechanism to improve the population diversity of BWO algorithm during the particle generation process at the outset of the algorithm, and introduces the operations of single-point crossover and diversity mutation during the iterative updating, to further enhance the local and global search ability, the detailed calculation steps are shown as follows:

(a) Identify the algorithm parameters, including the maximum number of iterations T_{max} and the overall size n.

(b) Oppositional learning strategy is used to generate the starting positions of all beluga whales and the fitness value can be acquired by the objective function. Oppositional learning strategy is shown in Equations (8) and (9):

$$X_i^j = l_i^j + \mathrm{rand}(0,1) \cdot \left(u_i^j - l_i^j\right) \#(8)$$

$$OX_i^j = l_i^j + u_i^j - X_i^j \#(9)$$

where X_i^j is the position of the whale in the algorithm;OX_i^j is the opposing point of X_i^j; u_i^j and l_i^j define the upper and lower bounds of the search range.

*(c)*In the exploration and exploitation phase, each whale decides which phase to enter. If $B_f > 0.5$, the update mechanism enters the exploration phase; if $B_f < 0.5$, the update is controlled by the exploitation phase. Subsequently, the current iteration's optimal value is found via computing and ranking the fitness values of the belugas' current position.

(d) Whale fall stage updates. During each iteration, the likelihood of a whale falling W_f also needs to be calculated.

(e) Particle crossover. To further enhance the algorithm's capabilities for local and global search and mitigate the occurrence of premature convergence during optimization, a particle crossover operation is introduced after the whale fall update. This involves selecting two chromosomes and splitting them at randomly chosen positions, then exchanging the right-hand segments to create two distinct sub-chromosomes. A schematic diagram of single-point crossover is illustrated in Figure 2.

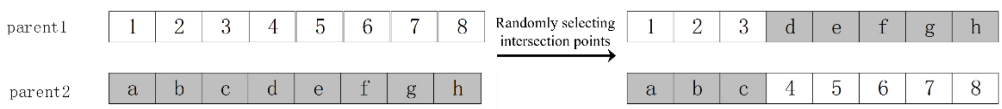

Figure 2 Single-point crossover schematic diagram

(f) Diversity mutation. After the particle crossover operation, to improve the global search capability, a diversity mutation operation is applied to the particle population. This involves randomly selecting an element $X_i = (x_{i1}, x_{i2}, \cdots x_{id})$ from an individual X_i with a probability of 1/d, then generating a random real number within the

range $[l_i, u_i]$ to replace the element x_{ik} in the individual, resulting in a new individual $X_i' = (x_{i1}', x_{i2}', \cdots x_{id}')$. This process is shown in Equation (10),

$$X_i' = \begin{cases} l_i + \lambda \cdot (u_i - l_i), i = k \\ X_i, \text{otherwise} \end{cases} \#(10)$$

where l_i and u_i is the upper and lower limits of the variable, and $\lambda \in [0,1]$ is a random number.

(g) The BWO algorithm stops when the current iteration exceeds the maximum iteration limit. Otherwise, repeat step (b).

Based on the above algorithm steps, the flowchart of the improved BWO (IBOW) is presented in Figure 3.

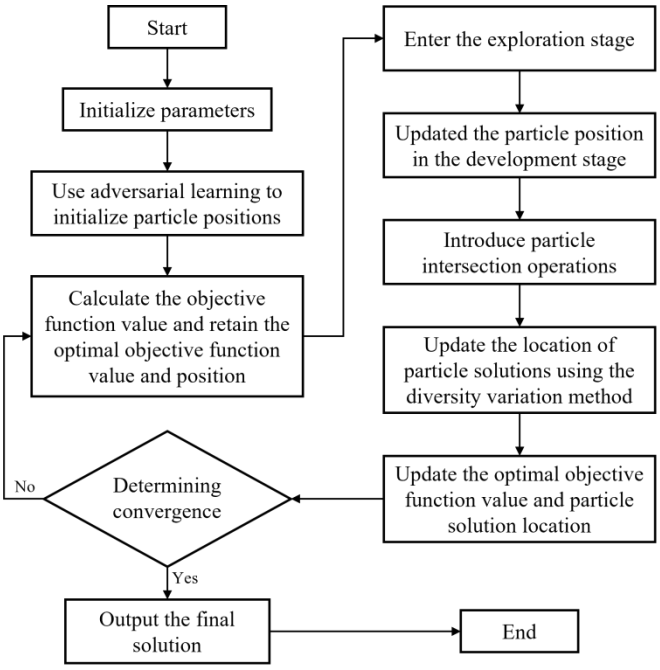

Figure 3 The flowchart of the IBWO algorithm

2.2.3 Temporal convolutional neural network - outcome forecasting

The Temporal Convolutional Network (TCN) is designed to address temporal sequence problems [40]. It possesses the capability to effectively extract the relationships between data points and make predictions about future data. Its primary architecture is based on dilated causal convolutions. What sets TCN apart from traditional Convolutional Neural Networks is its use of causal convolutions, which restricts it from having access to future data. This characteristic gives it a unidirectional structure, allowing it to infer future data solely from preceding data points. Consequently, TCN functions as a model that adheres to temporal constraints [41].

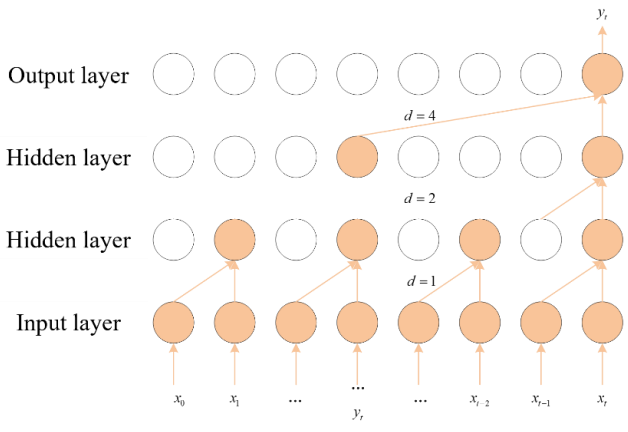

Figure 4 The dilated causal convolution structure of TCN

Dilated causal convolutions are illustrated in Figure 4. From the diagram, it is evident that the output y_t at time t can only depend on the inputs x_0 to x_{t-1} from earlier times. In this study, a TCN network with convolutional kernels of size 2 is employed, and dilation factors of d=1, 2, 4, and 8 are used.

The TCN network takes into consideration the temporal characteristics, and adjusts the length of output node memory according to different input time scales. This ability to adapt the memory length effectively addresses the issue of historical data forgetting present in traditional methods. As a result, TCN is more suitable for power prediction problems.

2.3 Wind and photovoltaic forecasting model based on ICEEMDAN-IBWO-TCN

Combined with the principle of the IBWO algorithm, we establishes a forecasting model based on the ICEEMDAN-IBWO-TCN algorithm to predicting the wind and photovoltaic power. The ICEEMDAN algorithm is applied to decompose the wind and photovoltaic power data to alleviate the impact of the volatility of wind and light data on the forecasting model, and the LSTM algorithm learns the features of the decomposed generated power results to realize the dynamic prediction of it. For the hyperparameters of the LSTM neural network, the IBWO algorithm optimizes the hyperparameters and select the optimal hyperparameter combination to enhance the accuracy and robustness. The flowchart of the forecasting model based on ICEEMDAN-IBWO-TCN algorithm is illustrated in Figure 5.

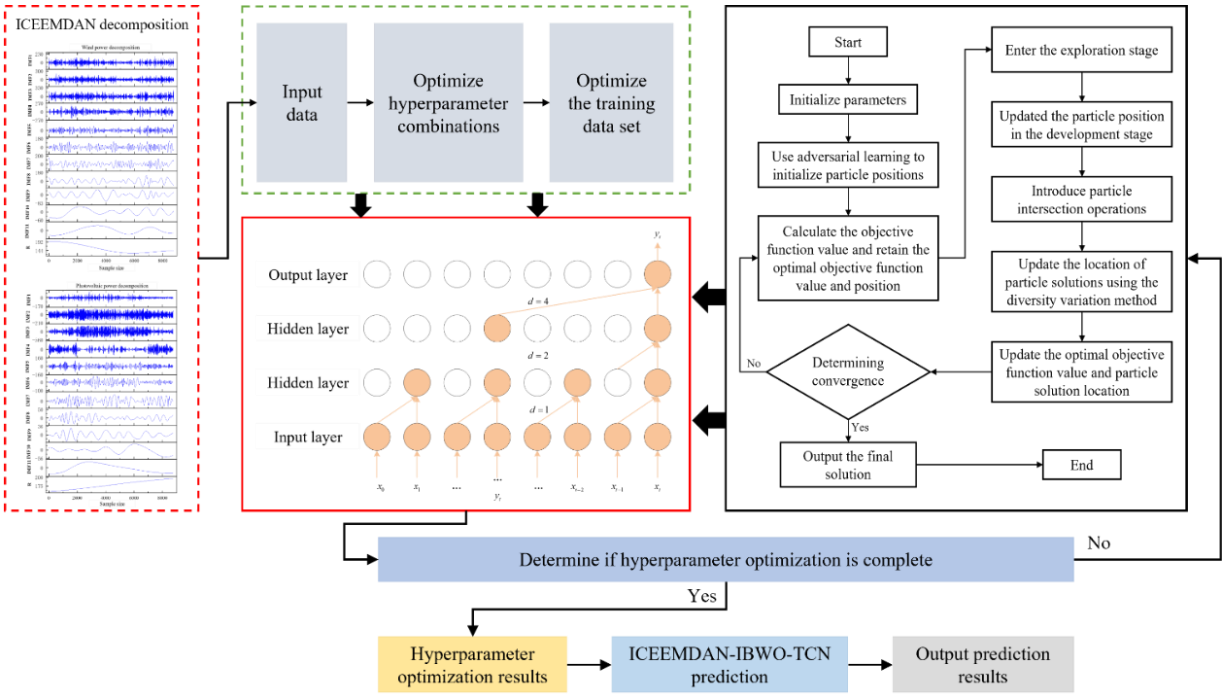

Figure 5 The flowchart of the forecasting model based on ICEEMDAN-IBWO-TCN

3. Results

3.1 Data

This paper takes the 2020 wind power and photovoltaic power data from an area in southern China, combined with the typical meteorological data of Jiangsu region in 2020 as the basis for data validation. The local wind power and photovoltaic power, related meteorological data and historical wind and photovoltaic power data are shown below in Figure 6.

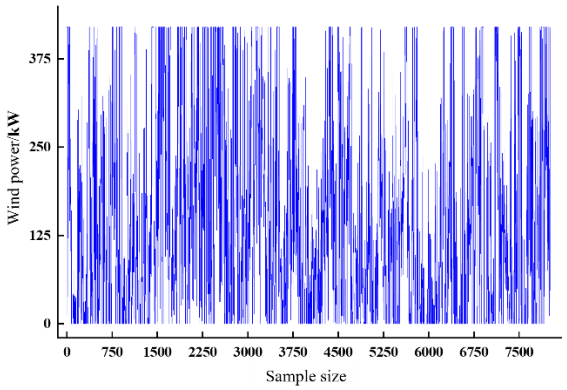

a) Wind power data.

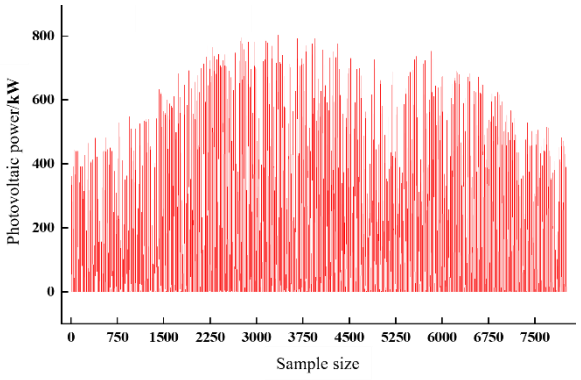

b) Photovoltaic power data.

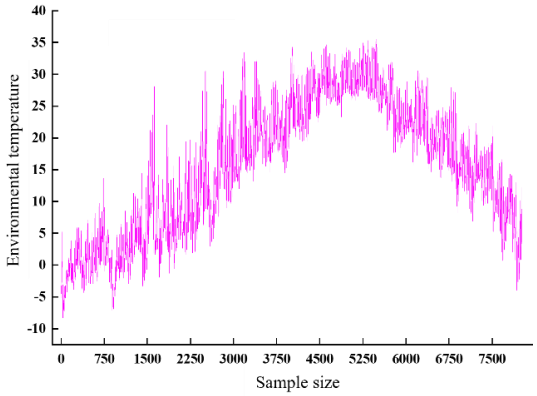

c) Environmental temperature data.

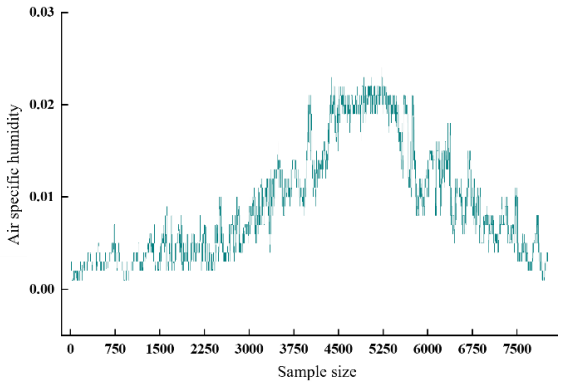

d) Air specific humidity data.

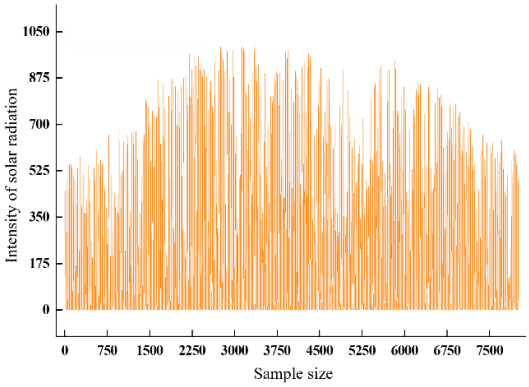

e) Intensity of solar radiation.

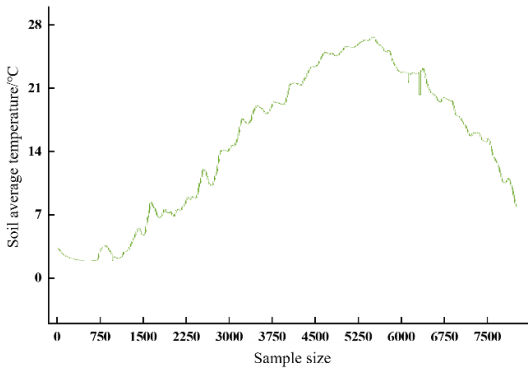

f) Soil average temperature data.

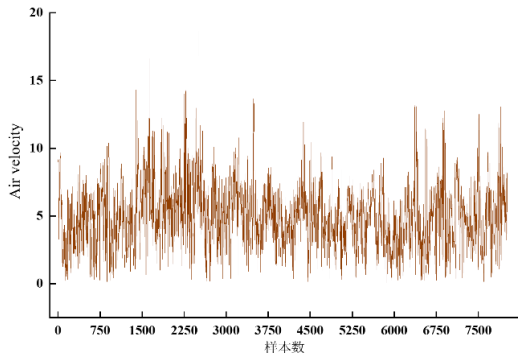

g) Air velocity.

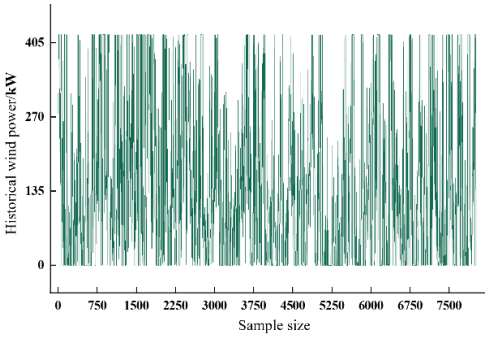

h) Historical wind power data.

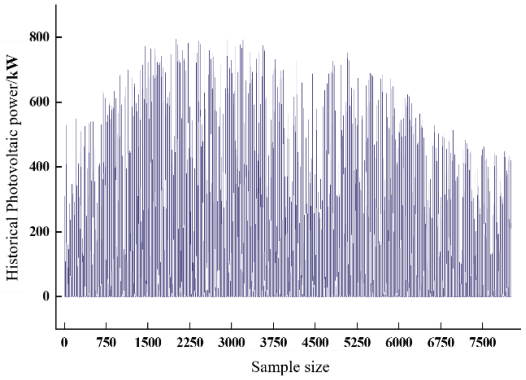

i) Historical photovoltaic power data.

Figure 6 Wind power and photovoltaic power data in 2020 of a region in southern China

3.2 Correlation analysis

According to the description in Section 2.1, the correlations between wind and photovoltaic power can be calculated, and the analysis results are presented in Figure 7.

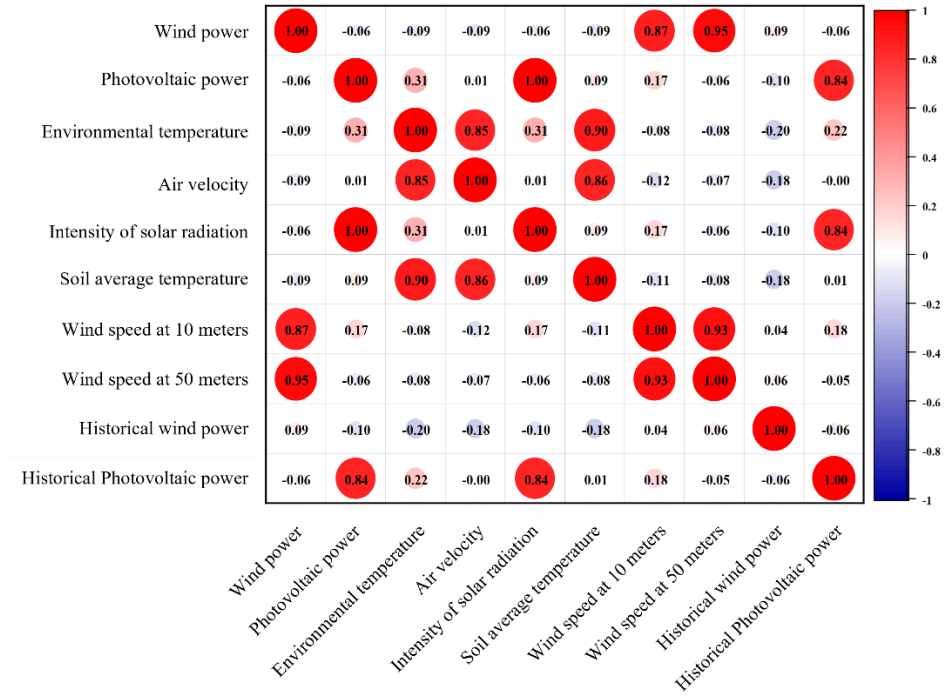

Figure 7 Wind and photovoltaic power correlation analysis results

Table 2 Input and output parameters of wind and photovoltaic power forecasting model.

Parameters	Wind power forecasting model	Photovoltaic power forecasting model
Input	Historical wind power Wind speed at 10 meters Wind speed at 50 meters	Environmental temperature Intensity of solar radiation Historical photovoltaic power
Output	Forecasted wind power	Forecasted photovoltaic power

Based on the results shown in Figure 7, it is evident that among the influencing factors for wind power, the wind speeds at 10 meters and 50 meters, as well as the historical wind power, exhibit high levels of correlation, all being indicators of strong correlation. The correlation analysis results of the other influencing factors are all below 0.3, indicating weak correlations. Regarding photovoltaic power influencing factors, historical solar power

and solar radiation intensity are both highly correlated factors, while the environmental temperature shows a moderate correlation with a correlation coefficient of 0.3. The correlation analysis results for the other influencing factors are all below 0.3, indicating weak correlations. In accordance with the evaluation criteria for correlation analysis, this study retains influencing factors with moderate or higher correlation coefficients on the input side of the forecasting model, and discards those with low correlation coefficients. This approach is taken to mitigate the impact of weakly correlated factors on wind and photovoltaic power prediction results. Consequently, the resulting input parameters for the forecasting models are presented in Table 2.

3.3 Forecasting results

We employ the ICEEMDAN algorithm described in Section 2.2 to mitigate the impact of the power fluctuations and complexity on prediction results. This algorithm decomposes wind and photovoltaic power into multiple relatively smooth intrinsic mode components, creating a set of component neural network forecasting models. Figure 8 depicts the power modal decomposition results.

The modal decomposition results are presented in Figure 8, it can be observed that the fluctuation of the first five intrinsic modal components is relatively large, but from the sixth intrinsic modal component, the fluctuation of the results of its intrinsic modal components is reduced and gradually smoothed, which has less effect on the precision of the forecasting model. According to the above decomposition results, combined with the wind and photovoltaic power forecasting model in section 2.2, the power forecasting results are obtained in Figure 9. It is evident that ICEEMDAN-LSTM can better realize the power prediction, but there is still a certain forecasting error.

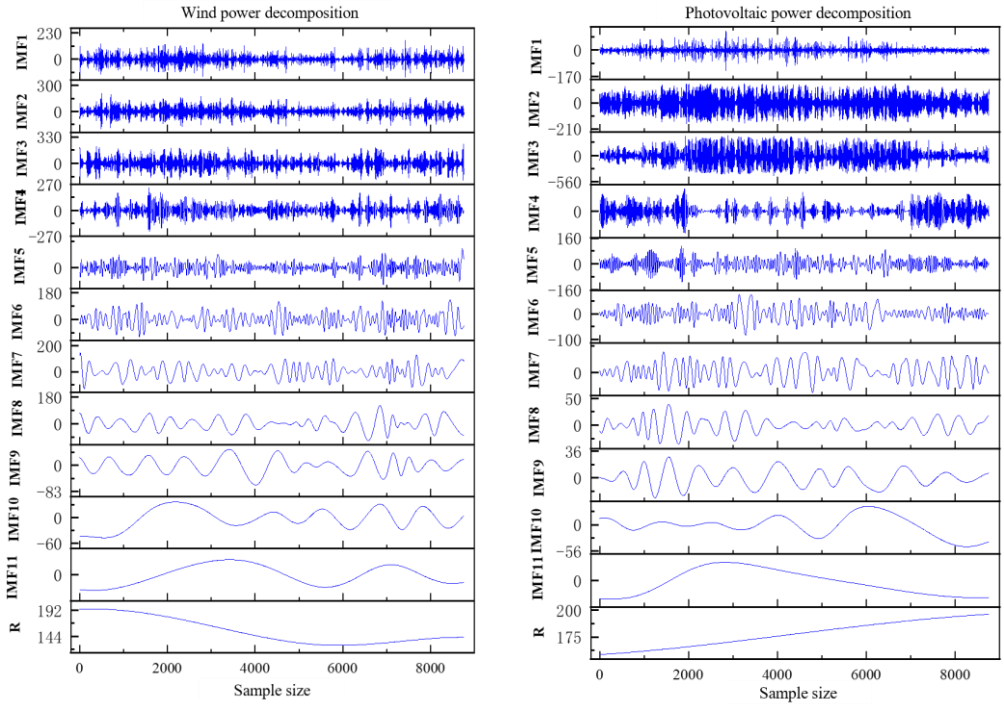

a) Wind power decomposition result. b) Photovoltaic power decomposition result.

Figure 8 Decomposition results

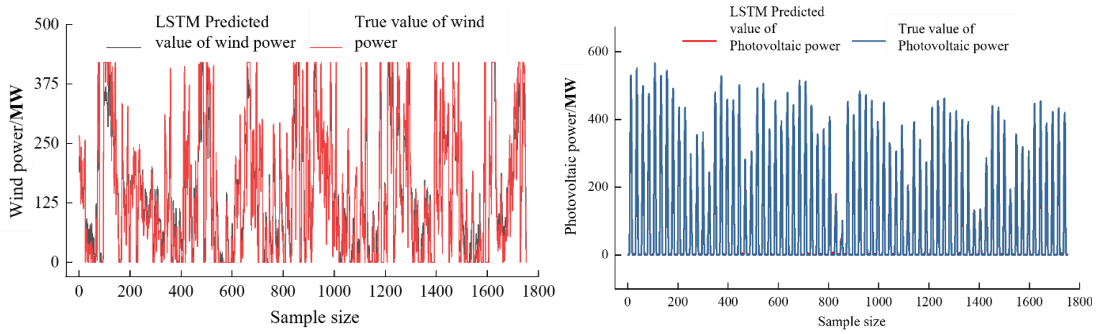

a) Wind power forecasting results. b) Photovoltaic power forecasting results.

Figure 9 Forecasting results based on ICEEMDAN-LSTM

Figure 10 shows the forecasting error in the test set, it is obviously that in the wind power forecasting, most of the errors are between [-55kW,55kW], and the peak error is relatively small. In the photovoltaic power forecasting, most of the errors are between [-4kW,4kW], and the prediction accuracy is high. Despite the relatively large error in wind power forecasting results, the order of magnitude of the forecasting error is relatively small compared to the wind power and is within the acceptable range.

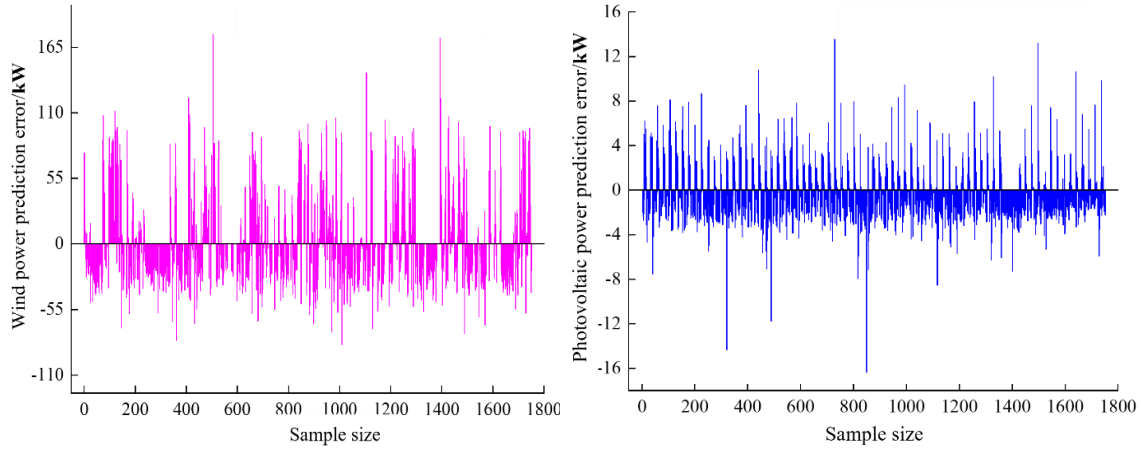

a) Wind power forecasting error. b) Photovoltaic power forecasting error.

Figure 10 The forecasting error based on ICEEMDAN-LSTM

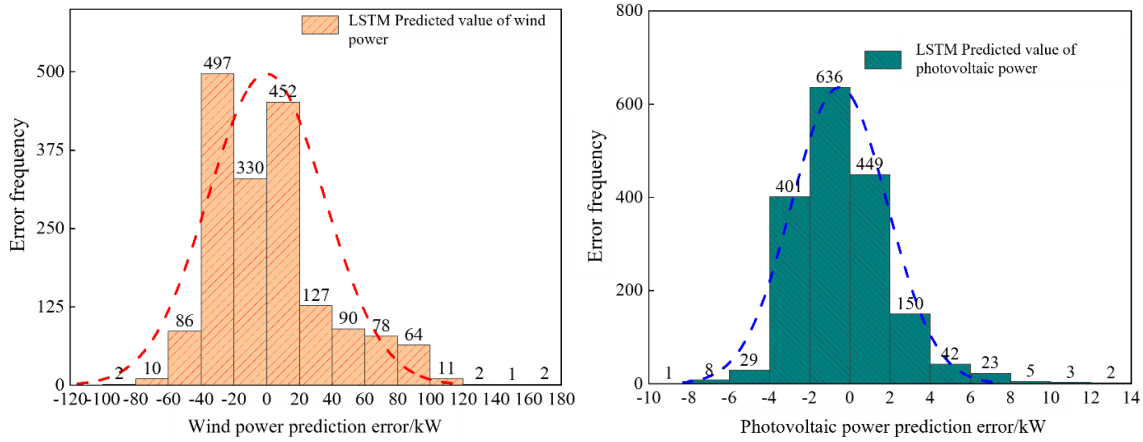

a) Wind power forecasting error distribution. b) Photovoltaic power forecasting error distribution.

Figure 11 Histogram of the forecasting error distribution

Through the error distribution histogram, we further analyze the prediction error results and the results were obtained in Figure 11.

The wind power forecasting error is mostly concentrated between [-40kW, 40kW], part of the error is between [-60kW, -40kW] and [40kW, 100kW], and only a small part of the error results are outside the range. Therefore, although there are some deviations between the predicted and actual wind power, it is still within the acceptable range, and its peak forecasting error is less, which can play a certain early warning role for the secure and stable functioning of the power grid.

It can be seen that most of the errors are in [-4kW,4kW] in the photovoltaic power forecasting results, and only a small part of the error is between [-10kW, -4kW] and [6kW, 10kW]. So the accurate forecasting of photovoltaic power can be realized by using ICEEMDAN-LSTM algorithm.

3.4 **Optimization of forecasting errors**

To enhance the power prediction accuracy while reducing the impact of renewable energy uncertainty on grid stability, this paper utilizes the ICEEMDAN-TCN algorithm to learn the features of the power forecasting errors, and realizes the dynamic error correction. Figure 12 illustrates the modal decomposition results of the forecasting errors.

As can be observed in Figure 12, starting from IMF5, the power forecasting error decomposition results are gradually smoothed, and the residual value curve has almost no fluctuation situation. After decomposition by ICEEMAN algorithm, the decomposed intrinsic modal component values are used to establish a component neural network prediction error trimming model, and utilize the TCN algorithm to realize the dynamic correction of wind power and photovoltaic power prediction error. Figure 13 shows the learning results of error characteristics.

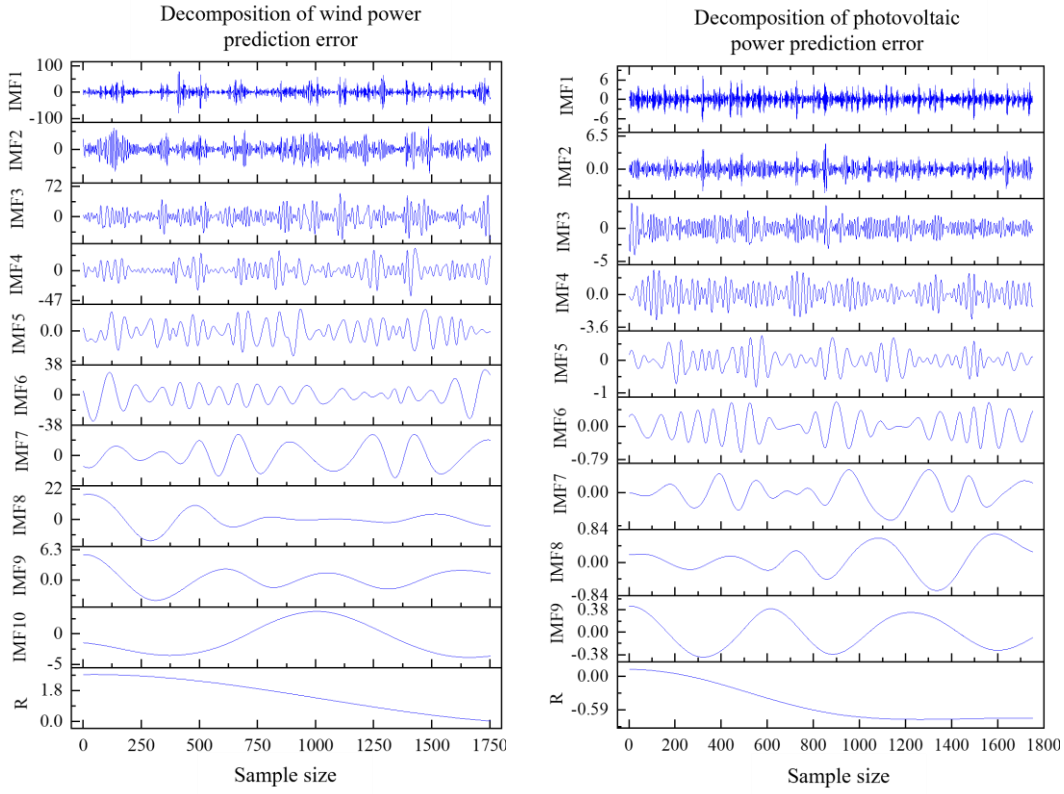

a) Wind power forecasting error decomposition result. b) Photovoltaic power forecasting error decomposition result.

Figure 12 The forecasting error decomposition results based on ICEEMDAN

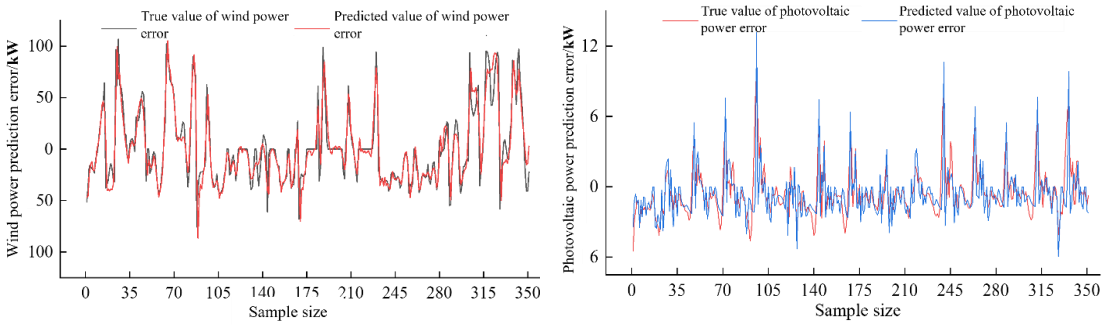

a) Comparison of wind power forecasting error result. b) Comparison of photovoltaic power forecasting error result.

Figure 13 Comparison of the power forecasting error results based on ICEEMDAN-TCN

According to the comparison results, the use of ICEEMDAN-TCN algorithm is able to better realize the error learning, and realize the accurate correction of the forecasting error of the wind and photovoltaic mobility rate, and provide a more reliable guarantee for the secure and steady functioning of the power grid.

4. Conclusions

This paper employs approaches such as deep learning prediction, data preprocessing and prediction error correction from the perspectives of meteorological and geographical factors to achieve accurate prediction of wind and photovoltaic power. And we using real-world data to validate the feasibility of the proposed methods. Firstly, weakly correlated factors are eliminated from the model's predictive outcomes through correlation analysis to improve predictions accuracy. Secondly, we utilize the ICEEMDAN-LSTM forecasting model. In the ICEEMDAN phase, the generated power is decomposed into several relatively smooth intrinsic mode components, reducing the impact of data volatility on forecasting results. During the LSTM network phase, multiple modal component neural networks are established, and reconstructing each modal component to obtain the prediction results of the forecasted wind and photovoltaic power. Lastly, constructing a power prediction error correction model to improve prediction accuracy. The research results are as follows:

(1) According to the correlation analysis, wind speed and historical power generation data effectively affect wind power. For photovoltaic power, the major influencing factors are solar radiation intensity, environmental temperature, and historical solar power data.

(2) The ICEEMDAN algorithm significantly reduces the impact of complexity and volatility of wind and photovoltaic power on prediction results. When combined with the powerful data mining and feature learning capabilities of the LSTM algorithm, it can achieve accurate forecasting of wind and photovoltaic power. This provides data support for subsequent low-carbon economic scheduling of the power grid, enhancing grid stability.

(3) The use of the time convolutional neural network achieves effective correction of prediction errors, significantly reducing peak errors and enhancing the robustness of wind and photovoltaic power prediction results.

References

[1] Y. Sun, W. Guan, Y. Cao, Q. Bao, Role of green finance policy in renewable energy deployment for carbon neutrality: Evidence from China, Renewable Energy 197 (2022) 643-653.

[2] Y. Zhang, C. Cheng, H. Cai, X. Jin, Z. Jia, et al, Long-term stochastic model predictive control and efficiency assessment for hydro-wind-solar renewable energy supply system, Applied Energy 316 (2022) 119134.

[3] X. Wang, X. Feng, T. Liu, Y. Lan, Y. Cui, A low-carbon economic dispatching for power grid integrated with wind power system considering right of using energy, Acta Energiae Solaris Sinica 41 (01) (2020) 255-263.

[4] M.S. Nazir, F. Alturise, S. Alshmrany, H.M.J. Nazir, M. Bilal, et al, Wind Generation Forecasting Methods and Proliferation of Artificial Neural Network: A Review of Five Years Research Trend, Sustainability 12 (9) (2020) 3778.

[5] M.S. Hossain, N. Abboodi Madlool, A.W. Al-Fatlawi, M. El Haj Assad, High Penetration of Solar Photovoltaic Structure on the Grid System Disruption: An Overview of Technology Advancement, Sustainability 15 (2) (2023) 1174.

[6] L. Lin, Y. Jia, M. Ma, X. Jin, L. Zhu, et al, Long-term stable operation control method of dual-battery energy storage system for smoothing wind power fluctuations, International Journal of Electrical Power & Energy Systems 129 (2021) 106878.

[7] C. Jiang, G. Xiong, J. Chen, J. Yang, J. Liang, Hybrid optimization method for dynamic environmental economic dispatch of wind-solar power system, Electric Power Science and Engineering 38 (09) (2022) 8-15.

[8] J. Kuang, Z. Lan, K. Yang, R. Guo, Distributed pumped storage location selection and optimal dispatch of multi-source power system containing wind, PV and hydropower, Energy Engineering 42 (04) (2022) 21-27.

[9] R. Ding, Maximum power point tracking method of photovoltaic system based on improved gray Wolf algorithm, Electronic Test 36 (22) (2022) 47-50.

[10] A. Couto, A. Estanqueiro, Enhancing wind power forecast accuracy using the weather research and forecasting numerical model-based features and artificial neuronal networks, Renewable Energy 201 (2022) 1076-1085.

[11] J. Ye, L. Xie, L. Ma, Y. Bian, X. Xu, A novel hybrid model based on Laguerre polynomial and multi-objective Runge–Kutta algorithm for wind power forecasting, International Journal of Electrical Power & Energy Systems 146 (2023) 108726.

[12] B. Yang, X. Yuan, F. Tang, Improved nonlinear mapping network for wind power forecasting in renewable energy power system dispatch, Energy Reports 8 (2022) 124-133.

[13] Y. Wang, H. Xu, R. Zou, L. Zhang, F. Zhang, A deep asymmetric Laplace neural network for deterministic and probabilistic wind power forecasting, Renewable Energy 196 (2022) 497-517.

[14] J. Wang, H. Guo, Z. Li, A. Song, X. Niu, Quantile deep learning model and multi-objective opposition elite marine predator optimization algorithm for wind speed prediction, Applied Mathematical Modelling 115 (2023) 56-79.

[15] Y. Wang, T. Chen, R. Zou, D. Song, F. Zhang, et al, Ensemble probabilistic wind power forecasting with multi-scale features, Renewable Energy 201 (2022) 734-751.

[16] J. Duan, M. Chang, X. Chen, W. Wang, H. Zuo, et al, A combined short-term wind speed forecasting model based on CNN–RNN and linear regression optimization considering error, Renewable Energy 200 (2022) 788-808.

[17] L. Yin, X. Cao, D. Liu, Weighted fully-connected regression networks for one-day-ahead hourly photovoltaic power forecasting, Applied Energy 332 (2023) 120527.

[18] G. Li, X. Wei, H. Yang, Decomposition integration and error correction method for photovoltaic power forecasting, Measurement 208 (2023) 112462.

[19] J. Liu, M. Cao, Z. Gao, K. Xu, A solar radiation prediction model based on radom forest Control Engineering of China 24 (12) (2017) 2472-2477.

[20] X. Zhao, Q. Li, W. Xue, Y. Zhao, H. Zhao, et al, Research on ultra-short-term load forecasting based on real-time electricity price and window-based XGBoost model, Energies 15 (19) (2022) 7367.

[21] V. Sharma, D. Yang, W. Walsh, T. Reindl, Short term solar irradiance forecasting using a mixed wavelet neural network, Renewable Energy 90 (2016) 481-492.

[22] C. Sun, X. Xu, Design of solar radiation illumination prediction system based on improved fruit fly algorithm, Modern Electronic Technology 44 (11) (2021) 83-86.

[23] L. Goliatt, Z.M. Yaseen, Development of a hybrid computational intelligent model for daily global solar radiation prediction, Expert Systems with Applications 212 (2023) 118295.

[24] G. Bi, X. Zhao, L. Li, S. Chen, c. Chen, Dual-mode decomposition CNN-LSTM integrated short-term wind speed forecasting model, Acta Energiae Solaris Sinica 44 (03) (2023) 191-197.

[25] D. Lu, X. Wang, X. He, Hybrid population particle algorithm and multi-quantile robust extreme learning machine based short-term wind speed forecasting, Power System Protection and Control 47 (05) (2019) 115-122.

[26] R. Yang, W. Li, Q. Bai, Y. Wang, X. Liu, et al, Signal-to-noise ratio improvement for BOTDA using CEEMDAN-WT method, Journal of Electronic Measurement and Instrument 36 (12) (2022) 28-36.

[27] B. Gao, X. Huang, J. Shi, Y. Tai, J. Zhang, Hourly forecasting of solar irradiance based on CEEMDAN and multi-strategy CNN-LSTM neural networks, Renewable Energy 162 (2020) 1665-1683.

[28] K. Zhu, Q. Fu, A photovoltaic power forecasting method based on EEMD-Kmeans-ALO-LSTM, Chinese Journal of Power Sources 47 (01) (2023) 103-107.

[29] Y. Yan, X. Wang, F. Ren, Z. Shao, C. Tian, Wind speed prediction using a hybrid model of EEMD and LSTM considering seasonal features, Energy Reports 8 (2022) 8965-8980.

[30] Z. Li, X. Luo, M. Liu, X. Cao, S. Du, et al, Wind power prediction based on EEMD-Tent-SSA-LS-SVM, Energy Reports 8 (2022) 3234-3243.

[31] T.H.T. Nguyen, Q.B. Phan, Hourly day ahead wind speed forecasting based on a hybrid model of EEMD, CNN-Bi-LSTM embedded with GA optimization, Energy Reports 8 (2022) 53-60.

[32] Y. Zhao, N. Guo, W. Chen, H. Zhang, B. Guo, et al, Multi-step ahead forecasting for electric power load using an ensemble model, Expert Systems with Applications 211 (2023) 118649.

[33] Y. Yu, X. Si, C. Hu, J. Zhang, A Review of Recurrent Neural Networks: LSTM Cells and Network Architectures, Neural Computation 31 (7) (2019) 1235-1270.

[34] Y. Li, B. Sun, J. Ding, S. Guan, Short-term wind-speed prediction of ocean surface based on LSTM, Marine Sciences 46 (11) (2022) 55-66.

[35] C. Hu, M. Xu, D. Hong, H. Wang, C. Liu, et al, Data-driven demand prediction based on integrated LSTM model, Electric Power Engineering Technology 41 (06) (2022) 193-200.

[36] C. Ji, C. Zhang, L. Hua, H. Ma, M.S. Nazir, et al, A multi-scale evolutionary deep learning model based on CEEMDAN, improved whale optimization algorithm, regularized extreme learning machine and LSTM for AQI prediction, Environmental Research 215 (2022) 114228.

[37] H. Cai, K. Hu, J. Li, X. Xin, Research on Fault Diagnosis and Location of Power Optical Cable Based on BWO-ELM Algorithm and VR-GIS Technology, Computer Measurement and Control 30 (12) (2022) 98-104+111.

[38] M.H. Nadimi-Shahraki, H. Zamani, Z. Asghari Varzaneh, S. Mirjalili, A Systematic Review of the Whale Optimization Algorithm: Theoretical Foundation, Improvements, and Hybridizations, Archives of Computational Methods in Engineering 30 (7) (2023) 4113-4159.

[39] H. Chen, Z. Wang, D. Wu, H. Jia, C. Wen, et al, An improved multi-strategy beluga whale optimization for global optimization problems, Mathematical Biosciences and Engineering 20 (7) (2023) 13267-13317.

[40] P. Lara-Benítez, M. Carranza-García, J.M. Luna-Romera, J.C. Riquelme, Temporal Convolutional Networks Applied to Energy-Related Time Series Forecasting, Applied Sciences 10 (7) (2020) 2322.

[41] R. Wan, C. Tian, W. Zhang, W. Deng, F. Yang, A Multivariate Temporal Convolutional Attention Network for Time-Series Forecasting, Electronics 11 (10) (2022) 1516.